6 Time-resolved studies of supramolecular assemblies of farnesylated hGBP1 in vitro

6.1 Introduction

Human Guanylate Binding Protein 1 (hGBP1) is a GTPase belonging to the family of dynamin-related proteins. Other members of this family like dynamin or bacterial dynamin-like protein (BDLP) are involved in membrane fission and fusion events for example[1]. A prerequisite for this functionality is the polymerization and membrane binding ability of those proteins. For BDLP it was shown that the inactive compact conformation is able to structurally rearrange and largely open a trunk region leading to a very elongated conformation that is polymerization competent[2]. Interestingly, these general fold properties like the globular GTP binding domain and the extended helical domain is conserved amongst eukaryotic dynamins even though their high sequence divergence.

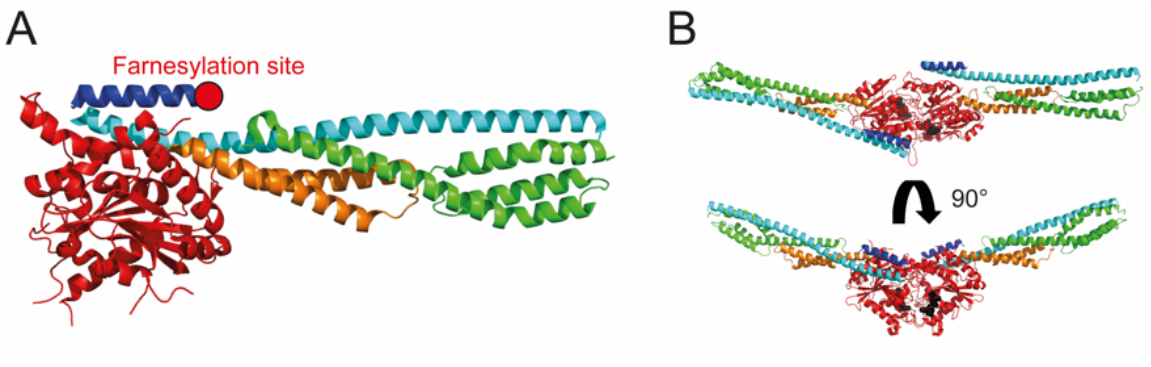

Figure 6-1: Crystal structure of unmodified hGBP1. (**A**) The C-terminal farnesylation site of hGBP1 is indicated with a red dot. Total length from the globular LG domain (red) to the extended end of the middle domain (orange/green) is approximately 125.3 Å. (**B**) Possible dimeric arrangement as proposed from the crystal structures of dimeric LG domains of hGBP1.

For hGBP1, this elongated structure was also observed in the crystal structure[3] (Figure 6-1) with the globular N-terminal domain (large GTPase/LG domain), a middle domain (MD) and the extended α helix 12, spanning the whole protein backbone of about 130 Å back to the LG domain, and C-terminal hydrophobic α helix 13, where the

farnesylation site is located. In previous experiments, hGBP1 was mainly studied in the non-farnesylated state, like the crystal structures available for the monomeric full-length protein[3,4] or for the monomeric and dimeric LG domain constructs[5]. But also functional and structural studies focused on unmodified hGBP1, drawing a picture of a hydrolysis cycle for GTP hydrolysis involving different oligomeric states of the protein, from monomeric in the inactive state to dimeric or even tetrameric in the nucleotide-bound and hydrolysis transition state respectively[6–8]. In our recent paper, we have moreover shown that the unmodified protein is able to largely rearrange upon nucleotide binding and comprises a high structural flexibility. This suggested rearrangement could lead to an additional interaction side as the C-terminal attached farnesyl is exposed and accessible for other extended molecules.

The first studies focusing on farn-hGBP1 *in vivo* have shown that it is mainly cytosolic but rearranges upon GDP AlFx addition for example to large vesicle-like structures as they were also observed for mGBPs (Figure 6-2). In a recent study using EM and vesicle binding assays, the authors have shown that farn-hGBP1 is able to form large supramolecular clusters[9] in contrast to the unmodified hGBP1 which forms dimers and eventually tetramers[8]. The protein assembly to 'supramolecular' complexes consisting of several thousand molecules has been shown to be essential to directly attack T. gondii for murine GBPs[10] (Figure 6-2).

In this study, we focused further on the polymerization behavior of farn-hGBP1. Using time-resolved SAXS measurements, we were able to follow the kinetics of assembly non-invasively in solution. With descriptive models, we have fitted the time course of assembly and built a kinetic model.

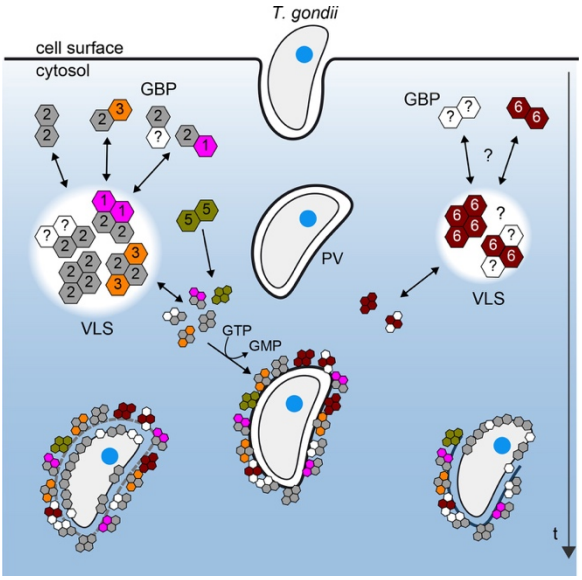

Figure 6-2: Schematic overview of mGBP multimerization upon T. gondii infection. Different isoforms of mGBPs are coded by different colors. Upon the assembly to vesicle-like structures (VLS), they are able to bind to parasitophorous vacuole membranes (PV). (adapted from Kravets et al. 2016[10])

6.2 Materials and Methods

6.2.1 Expression and purification of unmodified and farnesylated hGBP1

Unmodified and farnesylated hGBP1 were purified as described earlier[11,12]. In short, for expression of farnesylated hGBP1 (farn-hGBP1), the plasmid containing the hGBP1 gene was co-expressed with a plasmid coding for human farnesyltransferase subunits α/β. The plasmids were obtained from Dr. Gerrit Praefcke as a friendly gift and are the same as used in earlier publications and as the full-length protein used for crystallization[3,4]. Plasmids containing hGBP1 (pQE80L) and/or farnesyltransferase subunits α / β (pRSF-DUET1) were transformed in *E. coli* BL21(DE3)-RIL cells using the heat shock method, cultivated in Terrific Broth (TB) medium supplemented with 100 μg/ml ampicillin and/or 50 μg/ml kanamycin respectively and expression was induced by addition of 100 μM isopropyl β-D-thiogalactopyranoside. After 16 h at 22°C, cells were harvested by centrifugation at 5,000 x g for 20 min at 4°C.

Purification of hGBP1. Cells were resuspended in buffer containing 50 mM Tris-HCl (pH 7.9), 5 mM $MgCl_2$, 500 mM NaCl and 10% glycerol (v/v) and disrupted using a tip sonicator (Bandelin-Sonoplus) or a French pressure cell (Thermo Scientific) with a maximum pressure of 1.7 kbar at 4°C. After centrifugation at 15,000 *x* g for 60 min at 4°C, the supernatant was subjected to His_6-tag affinity chromatography (HisPur Cobalt Resin, Thermo Scientific, or TALON superflow, GE Healthcare). hGBP1 containing fractions were combined and ammonium sulphate was added to a final concentration of 3 M. After 10 min of stirring at room temperature, the precipitate was separated by centrifugation at 7,140 *x* g for 15 min at 4°C. The pellet was either stored at -80°C or directly resuspended in buffer C (50 mM Tris-HCl (pH 7.9), 5 mM $MgCl_2$, 150 mM NaCl) and applied onto a Superdex 200 26/60 column. All fractions containing monomeric hGBP1 were combined, concentrated to a final concentration of about 100 mg/ml and frozen in liquid nitrogen for storage at -80°C. The protein purity was analyzed by SDS-polyacrylamide gel electrophoresis (4-20% gradient gel, Expedeon).

Purification of farn-hGBP1. The purification strategy was the same as described for hGBP1, with an additional hydrophobic interaction chromatography (HIC, HiTrap Butyl HP, GE Healthcare) step for separation of unmodified from farnesylated hGBP1 after His_6-tag affinity chromatography. The HIC column was equilibrated with buffer containing high salt concentration (50 mM Tris-HCl (pH 7.9), 5 mM $MgCl_2$ and 1.2 M $(NH_4)_2SO_4$) and eluted with low salt buffer (50 mM Tris-HCl (pH 7.9), 5 mM $MgCl_2$). After His_6-tag affinity as well as after HIC chromatography, the protein containing fractions were precipitated using 3 M $(NH_4)_2SO_4$ as described for the unmodified hGBP1 before.

6.2.2 Sample preparation for further measurements

All buffers were degassed before usage and samples were freshly prepared directly before the respective measurements. Protein concentration was determined on a

NanoDrop 2000c Spectrophotometer (Thermo Scientific) using an extinction coefficient of 46340 M^{-1} cm^{-1} (calculated parameter of 1DG3.pdb, uniprot[13]).

The concentrated protein stock solution was diluted in buffer C (50 mM Tris-HCl (pH 7.9), 5 mM $MgCl_2$, 150 mM NaCl) or respectively buffer C with 300 μM $AlCl_3$ and 10 mM NaF to desired concentrations. Possible higher aggregates were removed by centrifugation at 13,400 x g for 22 min at room temperature (RT) and the supernatant was used for measurements. Nucleotides GDP and GTP were added directly before the measurement to final concentrations of 1mM.

6.2.3 DLS

Translational diffusion coefficients (D_{trans}) of the different samples were measured using dynamic light scattering experiments on a Malvern Zetasizer Nano ZS instrument (4 mW He-Ne laser, λ = 633 nm, θ = 173°). At least 15 runs per measurement were recorded to extrapolate the translational diffusion coefficient D_{trans} using the standard protein analysis mode of the instrument's software which is a non-negative least squares (NNLS) analysis followed by L-curve regularizer calculation.

6.2.4 Turbidity assays

Samples were prepared as described before and immediately after nucleotide addition placed in a cuvette holder at room temperature of a UV/Vis spectrophotometer (Thermo Scientific Nanodrop 2000c). The turbidity change after nucleotide addition was monitored at 350 nm.

6.2.5 Cryo TEM

Samples were prepared as described before and after different time points applied onto 200-mesh copper grids with Quantifoil R 2/2 holey carbon films (Quantifoil Micro Tools GmbH). The time point of polymerization kinetics was determined when the

sample was vitrified in liquid ethane using an automated vitrification robot (FEI Vitrobot Mark III) after blotting excess liquid. Prior to usage, TEM grids were surface plasma treated for 40 seconds using a Cressington 208 carbon coater.

EM pictures were taken with cryoTITAN operated at 300 kV of the Technische Universiteit Eindhoven/ FEI. It is equipped with a field emission gun (FEG), a post-column Gatan energy filter (GIF) and a post-GIF 2k x 2k Gatan charge-coupled-device camera.

Images were processed using ImageJ and a plugin called Radial Profile Angle. The particles to analyze were manually picked and the center for radial averaging placed at the darkest spot in the middle. Particles were usually averaged over 360° except for neighboring high density occurrences for example.

6.2.6 Fluorescence

A home-built microscopy setup at IPC/RWTH Aachen was used. Samples were prepared as described earlier, but additionally adding GDP ATTO-488 nucleotide in different amounts to desired concentrations as indicated in the results part. After nucleotide addition, samples were placed on a glass holder and covered with a coverslip to avoid drying effects. Images were recorded after indicated time points and processed using ImageJ.

6.2.7 SAXS measurements

All SAXS measurements were performed at ID02 at the European Synchrotron Radiation Facility (ESRF). A series of protein concentrations from 5 to 150 μM hGBP1 was measured. Each sample was dialysed against buffer C (50 mM Tris-HCl (pH 7.9), 5 mM $MgCl_2$, 150 mM NaCl) and dialysis buffer was measured before and after sample measurements for background subtraction. For stroboscopic measurements, the

acquisition time was optimized preventing protein aggregation and radiation damage to 0.01 to 0.5 s at room temperature. Different break durations between the acquisitions were chosen to cover a broad time range. The detector distance was varied from 1.5 to 30 m covering q ranges from 0.0484 to 5.1424 nm^{-1} (at detector distance 1.50 m), 0.0073 to 0.7642 nm^{-1} (at detector distance 10 m), 0.0035 to 0.3823 nm^{-1} (at detector distance 20 m) and 0.0021 to 0.2479 nm^{-1} (at detector distance 30 m).

6.2.8 SAXS data analysis

The scattering vector q is defined as $q = 4\pi/\lambda \cdot \sin(\theta/2)$ with the incident wavelength λ and scattering angle θ. The background subtraction was made using an averaged buffer file created using PRIMUS of the ATSAS suite and subtracted from all individual measurement files.

Simple geometric body fitting

Data were partly analyzed using a simple geometric model of a multi-shell cylinder. The form factor of the cylinder with 2 different electron density shells can be calculated as follows and was adapted for a multishell cylinder with 4 different layers, as implemented in the program jscatter[14]:

$$I(q)_{cylinder} = \frac{scale}{V_{shell}} \int_0^{\frac{\pi}{2}} f^2(q,\alpha) sin\alpha \, d\alpha \tag{6-1}$$

$$f(q,\alpha) = 2(\rho_{core} - \rho_{shell})\, V_{core}\, j_0(q\, H\, cos\alpha)\, \frac{J_1(q\, r\, sin\alpha)}{(q\, r\, sin\alpha)} + 2(\rho_{core} - \rho_{shell})\, V_{core}\, j_0(q\,(H + t)\, cos\alpha)\, \frac{J_1(q\,(r+t)\, sin\alpha)}{(q\,(r+t)\, sin\alpha)} \tag{6-2}$$

Initially free fit parameters were radii R1, R2, R3 and R4 with corresponding electron densities $\rho 1$, $\rho 2$, $\rho 3$ and $\rho 4$ and L as length of the cylinder. Radii and electron densities were determined from a global fit to the scattering data of highest farn-hGBP1 monomer concentration after addition of GDP AlFx at different time points and consecutively fixed for further data analysis. The electron density of the buffer was calculated using jscatter[14].

Interaction term / Correlation peak

A characteristic distance between scattering inhomogeneities leads to broad peak in the scattering pattern which can be described using the broad peak model as described by Hammouda.

$$I(q)_{broad\ Peak} = \frac{C}{1 + (|q - q_0|\ \xi)^m} + B \qquad (6\text{-}3)$$

The d-spacing is $q_0 = \frac{2\pi}{d_0}$, ξ is a correlation length, m is a Porod exponent and B and C are q independent constants obtained for $I(q\ \xi\ \to 0) = C + B$ and $I(q\ \xi\ \to \infty) = B$.

Modeling a linear combination of the populations

The whole fit was a linear combination of monomer, cylinder, power law scattering behavior and an interaction term.

$$\begin{aligned} I(q)_{fit} = \\ & A_{mon} \cdot I(q)_{mon} \\ & + A_{cylinder} \cdot I(q)_{cylinder} \\ & + I(q)_{broadPeak} \\ & + A_{polymer} \cdot q^{powLaw} \\ & + bgr \end{aligned} \qquad (6\text{-}4)$$

with

$$\chi^2 = \frac{1}{N - n_{param}} \sum_{i=1}^{N} \left(\frac{I(q_i)_{exp} - I(q_i)_{fit}}{w(q_i)} \right)^2 \qquad (6\text{-}5)$$

The populations are weighted by their respective pre-factors A. The scattering intensity of the monomer equals to the form factor of the crystal structure of hGBP1 (pdb ID 1DG3) and is calculated using Crysol from the Atsas package[15]. The scattering intensities of all other components are calculated as described before and are shown in Figure 6-3.

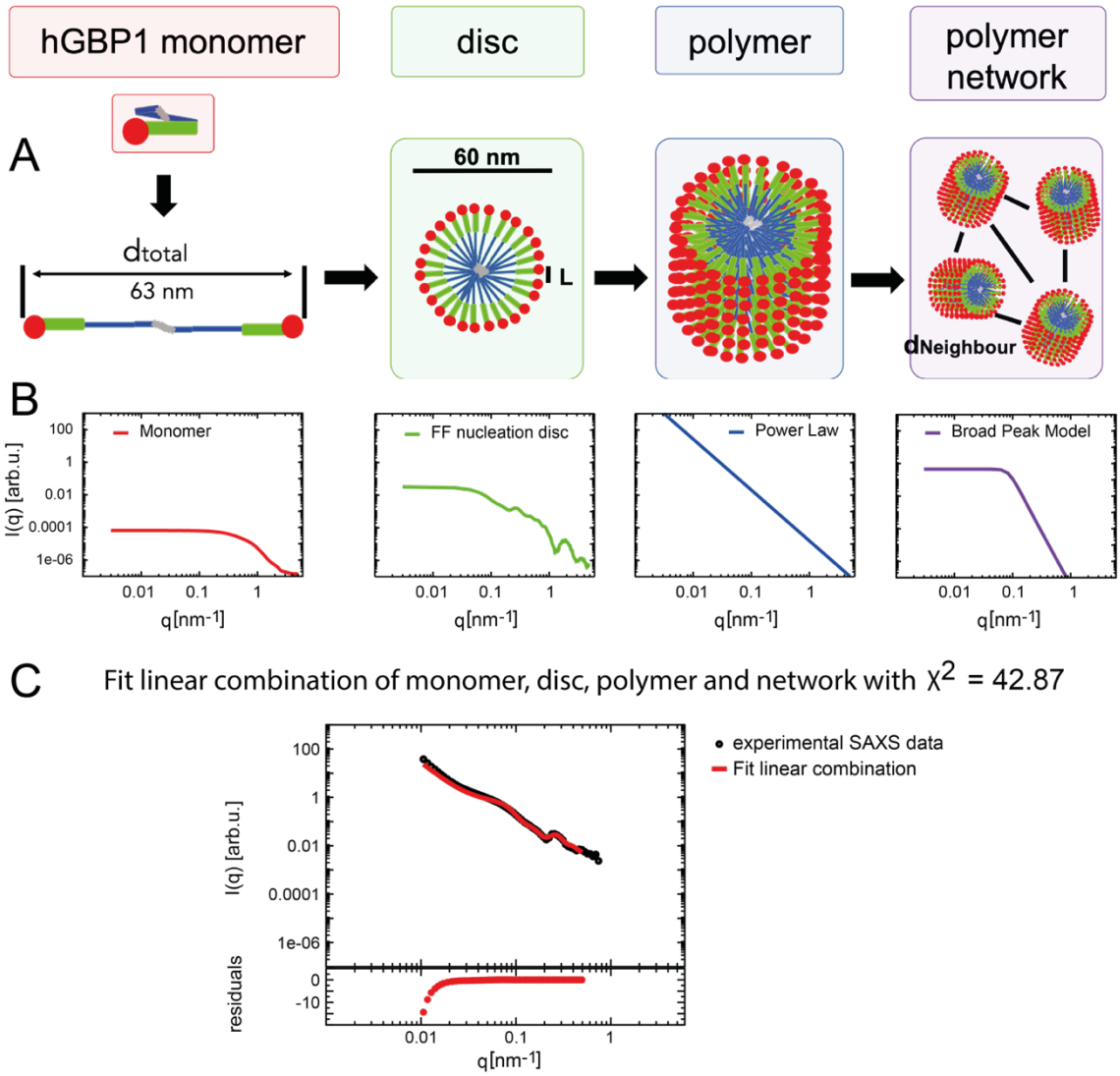

Figure 6-3: Schematic drawing of the linear combination of populations used to fit the TR-SAXS data. (**A**) Farn-hGBP1 monomer is shown with LG domain (red), MD (green), α-helical effector domains (blue) and farnesyl (grey) from N- to C-terminal. Hypothetical fully extended dimers shown with contact of farnesyl moieties, spanning in total a range of 63 nm. Discs are formed with LG domains on the outside and farnesyl in the inside, with a total diameter of about 60 nm from experimental measurements like EM and SAXS during polymerization. The discs further assemble to polymers consisting of the discs stacked in an unknown manner, the polymer term is described by power law behavior in the scattering experimental data. Upon built-up of polymers, a network is created with characteristic inter-polymer spacing termed $d_{Neighbour}$, which is described by the interaction term of the broad peak model in the linear combination. (**B**) Resulting form factors from components shown above. (**C**) Exemplary fit result (red) with linear combination model with above described populations of experimental data (black) is shown.

6.3 Results

6.3.1 Turbidity Assays

The earlier described polymerization of farn-hGBP1 in presence of nucleotides can be observed using turbidity assays. The transmittivity of the sample solution is followed at a wavelength of 350 nm in a regime, where neither protein or nucleotide are absorbing. The addition of 1 mM GTP leads after an initial lag time to a fast increase of turbidity. For this hydrolysable nucleotide, the turbidity disappears at later timepoints and the signal vanishes back to the initial background signal.

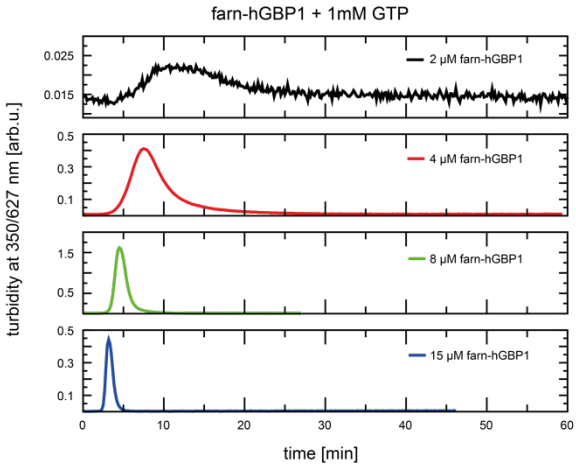

Figure 6-4: Turbidity assay of farn-hGBP1 in varying protein concentrations after addition of 1 mM GTP.

In the other case of GDP AlFx, which is a nucleotide trapping the protein nucleotide complex in the hydrolysis transition state, the turbidity onset is also delayed, defined as a lag time in the beginning. The observed turbidity change is irreversible over the whole detected time range. Even after several hours to days, the signal does not change except for sedimentation taking place after a while. Under both nucleotide conditions, the kinetics followed by turbidity change are protein concentration dependent.

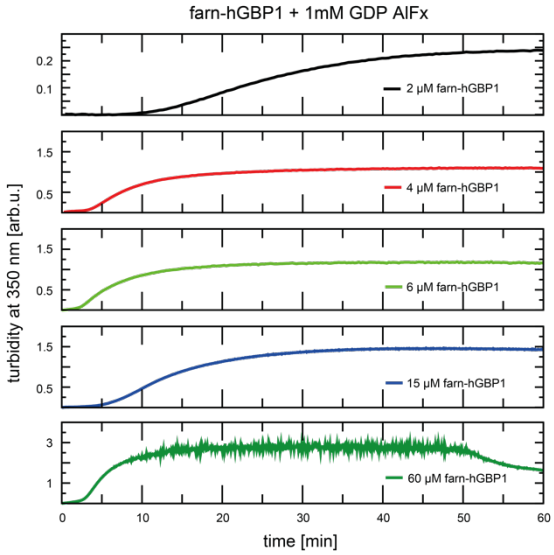

Figure 6-5: Turbidity assay of farn-hGBP1 in varying protein concentrations after addition of 1 mM GDP AlFx.

6.3.2 DLS

Following dynamic light scattering (DLS) experiments confirmed the appearance of higher oligomers and supramolecular structures. Directly after addition of 1 mM GTP (Figure 6-6), the hydrodynamic radius determined from the measured translational diffusion coefficient corresponds to about 3-9 nm representing a compact conformation of farn-hGBP1 before activation, as the crystal-like structure would yield a hydrodynamic radius of about 4 nm (calculated from pdb ID 1DG3 using hydropro) or 5.7 nm for a theoretical dimer as shown in Figure 6-1 (calculated from the dimer model using hydropro). After several minutes upon addition of GTP, a second species appeared with hydrodynamic radii of 200 – 600 nm. The apparent radius is first increasing and after a maximum of about 600 nm after around 40 min decreasing again to around 3-4 nm, probably indicating the complete reversion back to the monomeric protein after GTP hydrolysis (Figure 6-6).

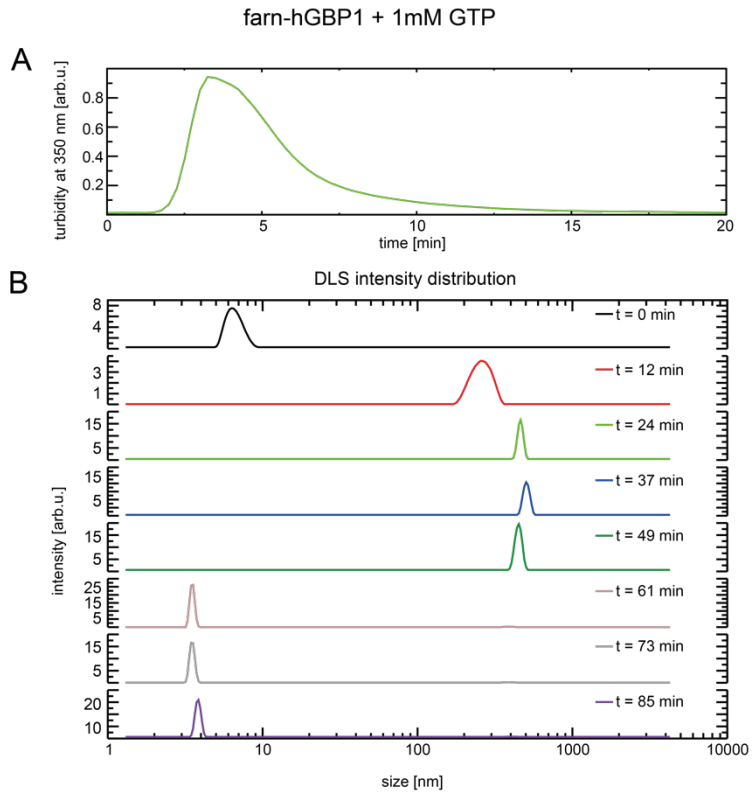

Figure 6-6: Turbidity change of farn-hGBP1 after GTP addition monitored at 350 nm in the upper panels. (**A**) Turbidity assay of 6 μM farn-hGBP1 after addition of 1 mM GTP (green). (**B**) DLS size distribution of 6 μM farn-hGBP1 with 1 mM GTP weighted based on intensities of the species, respectively shown at different timepoints as indicated in the legend.

After addition of GDP AlFx, additional oligomers next to the monomeric farn-hGBP1 appear with hydrodynamic radii around 20 nm and another species around 300-700 nm (Figure 6-7). In contrast to polymerization in presence of GTP, the additional species are observed with rather constant size and up to several hours. This would also confirm the observation of the turbidity assays, where the kinetics appear to be reversible in the case of GTP and irreversible for GDP AlFx.

The limits of DLS measurements are important to keep in mind as they are self-correlated data traces over a certain time interval, about 1 min intervals for most of the performed measurements, the polymerization probably takes place during the measured interval and perturbs the accuracy of size determination. Moreover, in the size regime of several hundreds of nanometers, light scattering is angle dependent (Mie scattering) and

the usually applied approximations for automated DLS data analysis do not hold anymore. Therefore, exact size estimations are not possible for these experiments, but they are still valuable information on the overall polymerization behavior of farn-hGBP1 induced by GTP or GDP AlFx respectively.

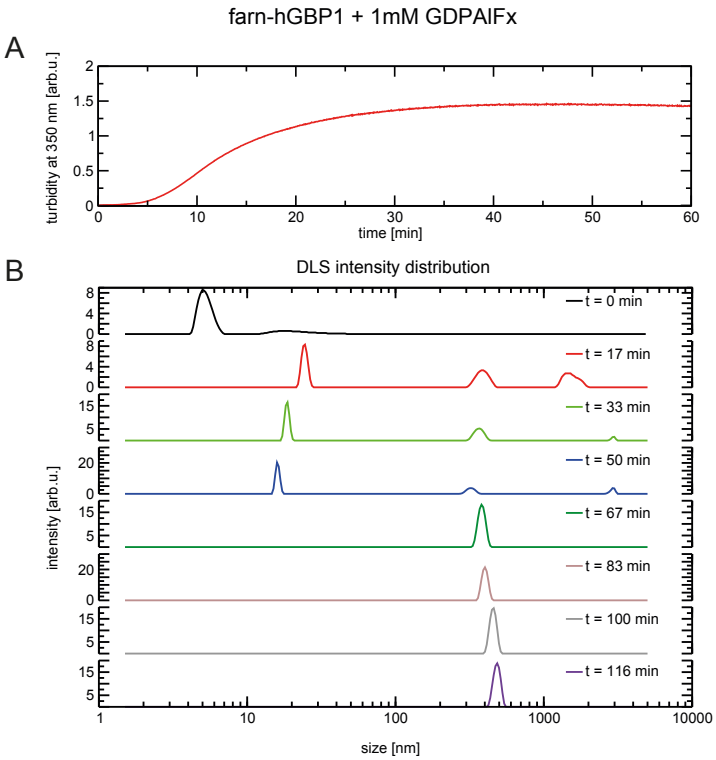

Figure 6-7: Turbidity change of farn-hGBP1 after GDP AlFx addition monitored at 350 nm in the upper panels. (**A**) Turbidity assay of 15 μM farn-hGBP1 after addition of 1 mM GDP AlFx (red). (**B**) DLS size distribution of 14 μM farn-hGBP1 with 1 mM GDP AlFx weighted based on intensities of the species, respectively shown at different timepoints as indicated in the legend.

6.3.3 Cryo TEM

The observed polymerization was also studied using cryo electron microscopy for more reliable size information compared to DLS for the reasons explained before. The samples were plunge frozen at different time points after nucleotide addition, thereby allowing to follow the structural changes during polymerization. From the lowest

magnification (6.5k), a different extent of aggregation can be observed between 29-899 seconds (Figure 6-8). At the first timepoint (29 s), the water filled hole in the grid seems to contain only a layer of vitrified water with a constant background density, implying that the protein and nucleotides contained in the sample are randomly distributed. After 122 seconds, first shadowed regions can be observed. The regions span from the carbon grid across the water filled hole and seem to be interconnected. The network expands further as observed at later timepoints like 319, 466 and 899 seconds, covering almost the whole grid surface at later timepoints.

Interestingly, the structures observed at higher magnifications are mainly disc-like particles with varying contrasts at different radial positions. The disc-like structures are mainly observed perpendicular to the beam direction or slightly twisted, allowing to calculate a density profile. The discs also attach to each other in some observations, mediated by the outer leaflet. Stacked discs as proposed by Shydlovskyi et al.[9] are very rarely observed and not representative for the observations made in this experiment.

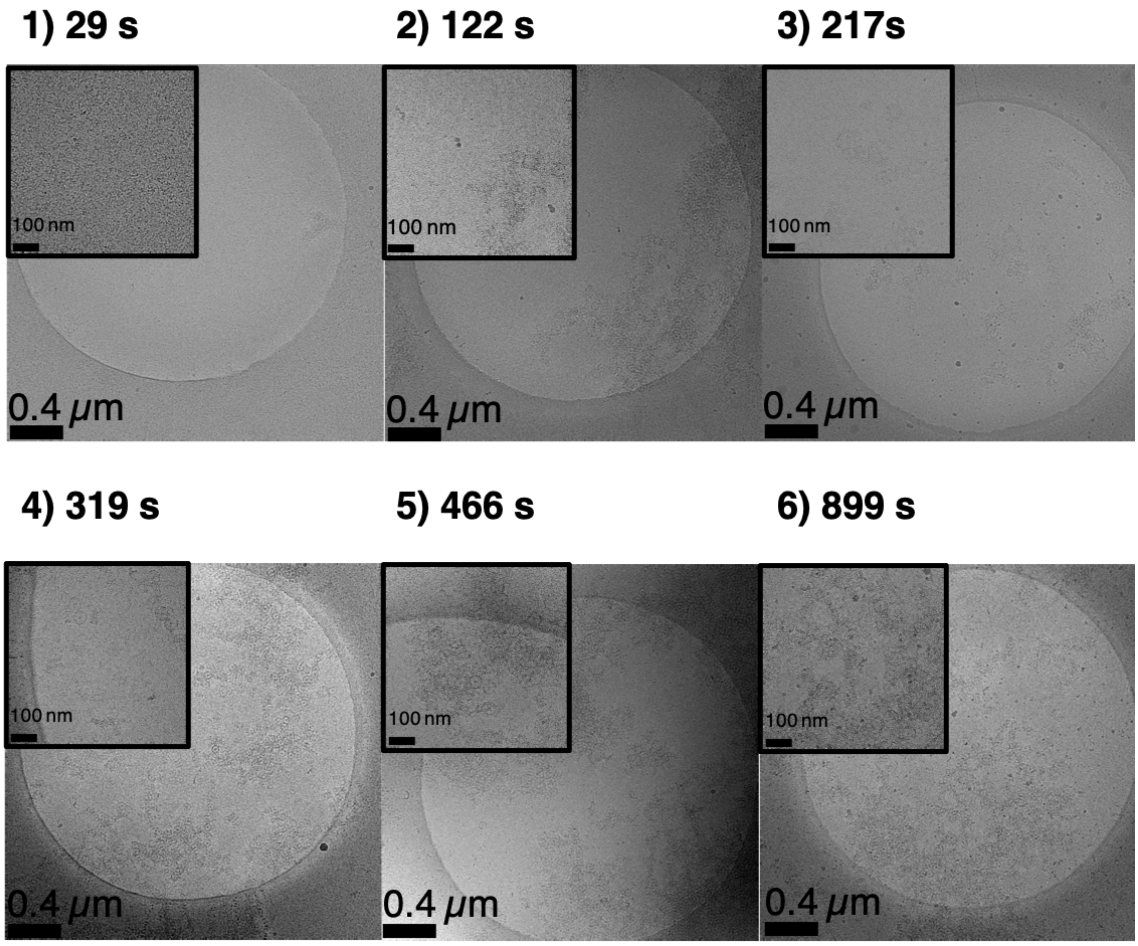

Figure 6-8: Cryo TEM images of farn-hGBP1 (30 μM) at different timepoints after GDP AlFx (1 mM) addition. Grid overview images at 6.5 k magnification (Scale bar 0.4 μm) with insets of higher magnification (24k, scale bar 0.1 μm).

By picking the disc-like structures observed at the two magnifications and radially averaging their density profiles, one dimensional length profiles are created (Figure 6-9). The obtained contrast profile could be used for distance refinement of the disc layers that are used for fitting the SAXS data, as described earlier.

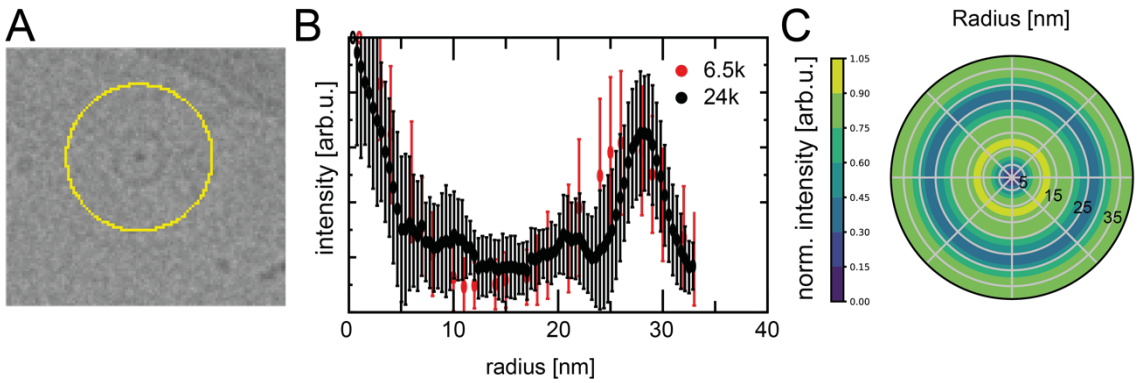

Figure 6-9: Disc-like nanostructure evaluation scheme. (**A**) First, disc-like structures in the pictures obtained are manually picked and the center of a circle around the particles is placed at the darkest spot in the middle of the disc. (**B**) The circles drawn in step A are radially averaged and plotted after averaging of singular one-dimensional traces (n = 125 for 6.5k magnification, n = 18 for 24k magnification). (**C**) The one-dimensional density contrast plot is schematically presented as 2D disc with varying density indicated by color intensity.

6.3.4 SAXS

To gain insights into the inner structure of the observed discs, SAXS and USAXS was performed. The scattering pattern over time was recorded after addition of the nucleotides as described before at various detector distances varying thereby the observed q range and in consequence the observable length scale of the structures.

After addition of 1 mM GTP, changes in the scattering pattern can be observed at all detector distances (Figure 6-10). The observed changes are reversible over the measured time range, showing that the first and the last measured time point (after 90 s and after 515 s respectively for 35 μM farn-hGBP1, Figure 6-10) are virtually the same. A peak in the scattering pattern is appearing after approximately 185 s at around 0.25 nm^{-1}, but also an upturn in forward scattering direction can be observed (< 0.1 nm^{-1}). At the next measured detector distance of 10 m, covering a q range of 0.01 to around 0.8 nm^{-1}, similar effects are observed. A peak around 0.25 nm^{-1} arises after around 180 s and the upturn in forward scattering direction evolves to a steeper slope. A new observation is the appearance of a second plateau at small angles that can be observed in the beginning (around $0.01 - 0.02$ nm^{-1}, Figure 6-10). This could be due to species of

higher molecular weight that are already built after 141 s, but as the smaller detector distance shows a full turn-over of farn-hGBP1 monomers that are present in the beginning back to monomers after GTP hydrolysis, it is more likely that the background subtraction is not precise enough at higher detector distances and due to the very low scattering intensity of the small biomolecules. This upturn is therefore regarded as experimental artefact and not further discussed anymore. The return of the scattering pattern to the initial condition confirms the earlier observed reversible kinetics from turbidity and DLS experiments in presence of GTP.

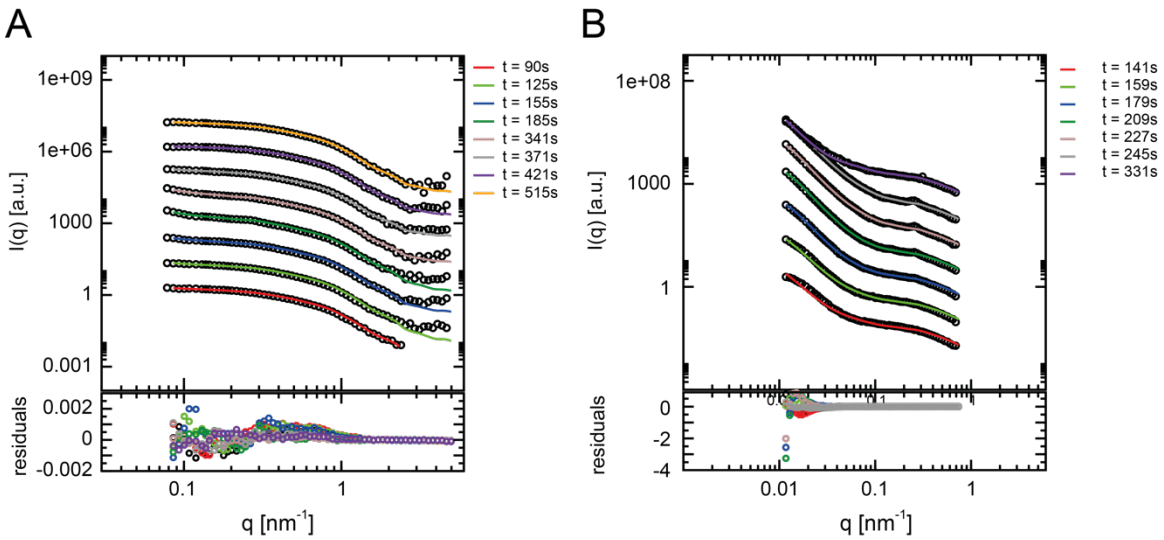

Figure 6-10: Time resolved SAXS measurements of 35 μM farn-hGBP1 after addition of 1 mM GTP. (**A**)/(**B**) Experimental raw data at detector distance of 1.5 m or 10 m respectively are shown with different time points being color coded according to the scheme on the right of the plot. Experimental data are plotted in black with the linear combination of the populations fitted to the data at different time points in different colors. The residual deviation of the fits from the experimental data is shown in the panel below.

In the case of kinetics observed after GDP AlFx addition, the scattering intensity changes during the time course but stays constant after a certain time (Figure 6-11). This observation matches well with the non-reversible polymerization kinetics as described before for turbidity and DLS measurements. Scattering at high q values stays constant after approximately 4 minutes (Figure 6-11 A and C), implying that the inner structure is readily formed in a first phase. After this first phase, changes in the scattering pattern are observed in the low q range at larger detector distances (Figure

6-11 B and D). This points to the assumption that only structural reassembly on a macromolecular level takes place and that the inner structure of the assembled polymer is similar to the soluble precursors. After more than 10 minutes, the scattering pattern does not observably change even at lowest q values.

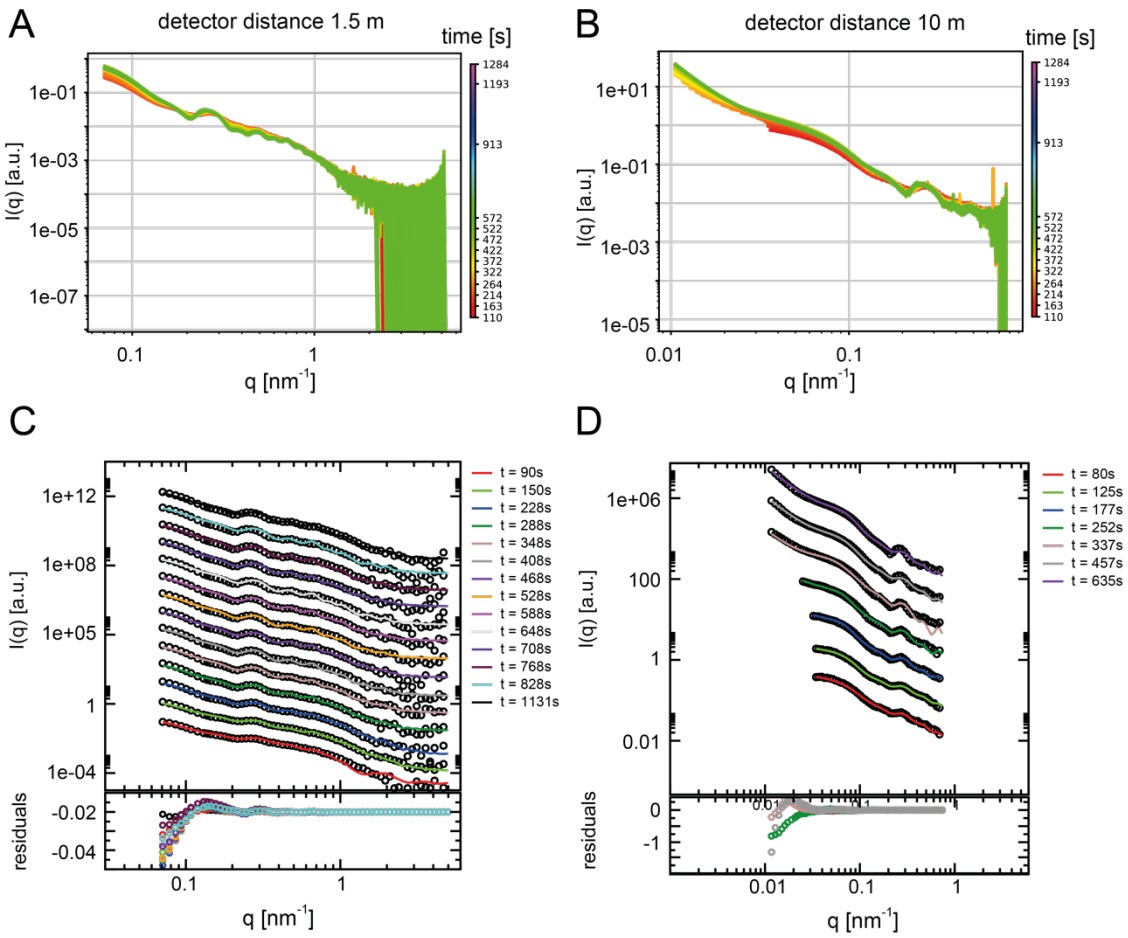

Figure 6-11: Time resolved SAXS measurements of 15 μM farn-hGBP1 after addition of 1 mM GDP AlFx. (**A**)/(**B**) Experimental raw data at detector distance of 1.5 m or 10 m respectively are shown with different time points being color coded according to the scheme on the right of the plot. (**C**)/(**D**) Representative raw data of the upper panels (A) and (B) are plotted in black with the linear combination of the populations fitted to the data at different time points in different colors. The residual deviation of the fits from the experimental data is shown in the panel below.

6.3.5 Fluorescence imaging

Using fluorescence imaging, the earlier observed unspecific aggregation in electron microscopy images can be confirmed. With GDP AlFx, the network appears to be evenly distributed throughout the observation window (Figure 6-12 A). In presence of GTP, a network comprising differently sized wholes can be observed (Figure 6-12 B).

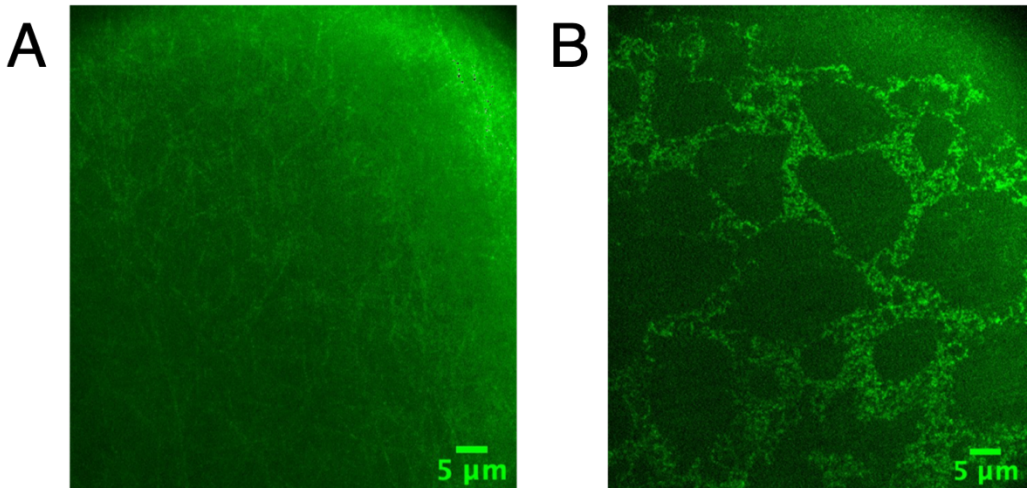

Figure 6-12: Fluorescence imaging of farn-hGBP1 polymer networks after nucleotide addition. (**A**) Networks of 300 μM farn-hGBP1 after addition of 1mM GDP with 0.1 μM GDP-ATTO488 in buffer containing AlFx. (**B**) Networks of 2 μM farn-hGBP1 after addition of 1mM GTP and 0.1 μM GDP-ATTO488.

6.3.6 Comparison of kinetics from different methods

The time-dependent parameters obtained from SAXS data fitting are compared to the earlier obtained macroscopic observations from turbidity assays as well as from cryo TEM obtained information about the discs in solution.

For farn-hGBP1 in presence of GTP, measurements at 6 μM protein concentration are very low in scattering intensity and the signal can therefore not be extracted easily. For turbidity assays on the other hand, concentrations as needed for SAXS were challenging due to the fast onset of the kinetics and the high turbidity signal, leading to early detector saturation. Therefore, in Figure 6-13, the kinetic profile of 6 μM farn-hGBP1 with GTP in a turbidity assay is compared to the amplitudes obtained for

monomer scattering and disc scattering from SAXS experiments at 63 μM farn-hGBP1 with GTP. The monomer signal follows a similar trend at both measured detector distances and therefore size ranges, showing a short lag time during the first 120 seconds, leading to a fast decay of the signal and a slow recovery that is not fully resolved in the time course of measurements (Figure 6-13 C). The signal of the discs on the other hand, is better described at higher detector distances, meaning on larger length scales (Figure 6-13 D). Comparable to the onset of monomer decay, an upturn of the disc scattering intensities is observed. The polymer scattering contribution was only fitted for detector distances higher than 1.50 m, as the relevant scattering regime is not recorded at the higher q values. The polymer scattering follows the kinetics similar as the observed turbidity change, implying that the turbidity is mainly due to polymer scattering contributions.

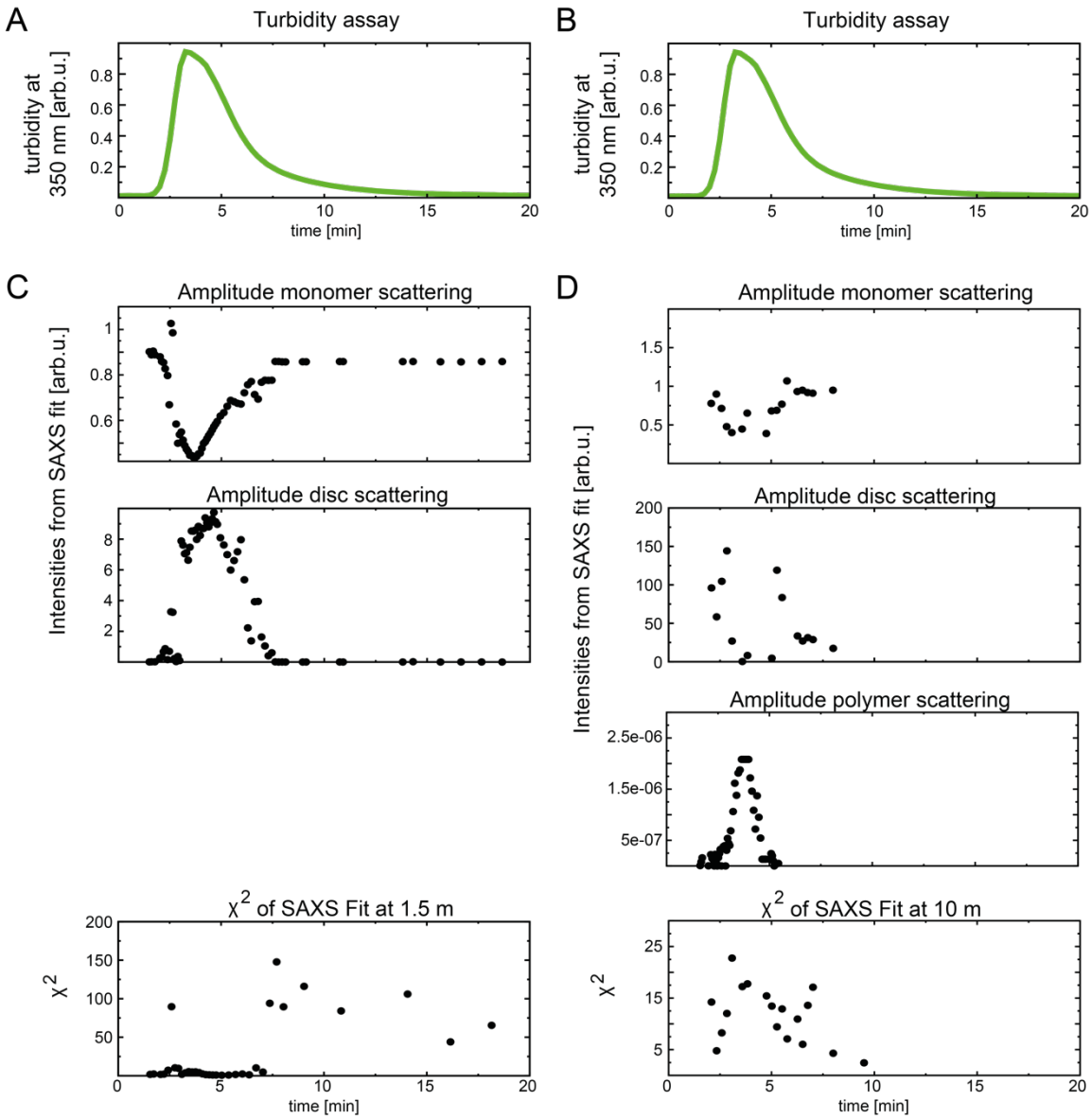

Figure 6-13: Comparison of time-dependent changes in turbidity experiments and of SAXS fit parameters obtained from linear combination of populations model. (**A**)/(**B**) Turbidity change of farn-hGBP1 after nucleotide addition monitored at 350 nm in the upper panels. Both showing 6 μM farn-hGBP1 with 1 mM GTP in green. (**C**) Amplitude changes of the components included in the SAXS fit to describe the experimental data of 63 μM farn-hGBP1 with GTP at a detector distance of 1.50 m. Upper panel is showing amplitudes of the monomeric protein and in the second row of the disc-like structures. Last row is indicating the χ^2 values of the fit results. (**D**) Amplitude changes of the components included in the SAXS fit to describe the experimental data of 63 μM farn-hGBP1 with GTP at a detector distance of 10 m. Upper panel is showing amplitudes of the monomeric protein, second row of the disc-like structures and third row for polymer scattering contributions. Last row is indicating the χ^2 values of the fit results.

The polymerization of farn-hGBP1 in presence of GDP AlFx is shown in Figure 6-14. At the lowest SAXS detector distances, the decay of monomer signal coincides very well with the upturn of disc-like particles. Moreover, at 10 m, the formation of polymers is observed on a similar time scale as for the disc-like particles. At the highest detector distance, only a snapshot at a late polymerization state was taken which can only be used to confirm the presence of polymers seen at lowest q values. Even though the q range down to 0.004 nm^{-1} was measured, a plateau region was not reached, thereby preventing the structural characterization or determination of overall parameters like radius of gyration for these polymers is prevented.

Interestingly, the kinetics observed in the SAXS experiments are faster compared to the bulk measurement by turbidity, as even the onset of polymerization is taking place during the lag phase of turbidity and a plateau of polymers is reached earlier as in turbidity assays. The same was observed in the presence of GTP, as the turbidity assays of 6 μM farn-hGBP1 show similar time constants compared to 63 μM farn-hGBP1 SAXS measurements. This effect could be due bad mixing the turbidity cuvettes, as the small nucleotide volume was carefully added to the cuvette avoiding bubbles or shaking. Therefore, diffusion effects might be responsible for the late onset of polymerization in UV/Vis experiments.

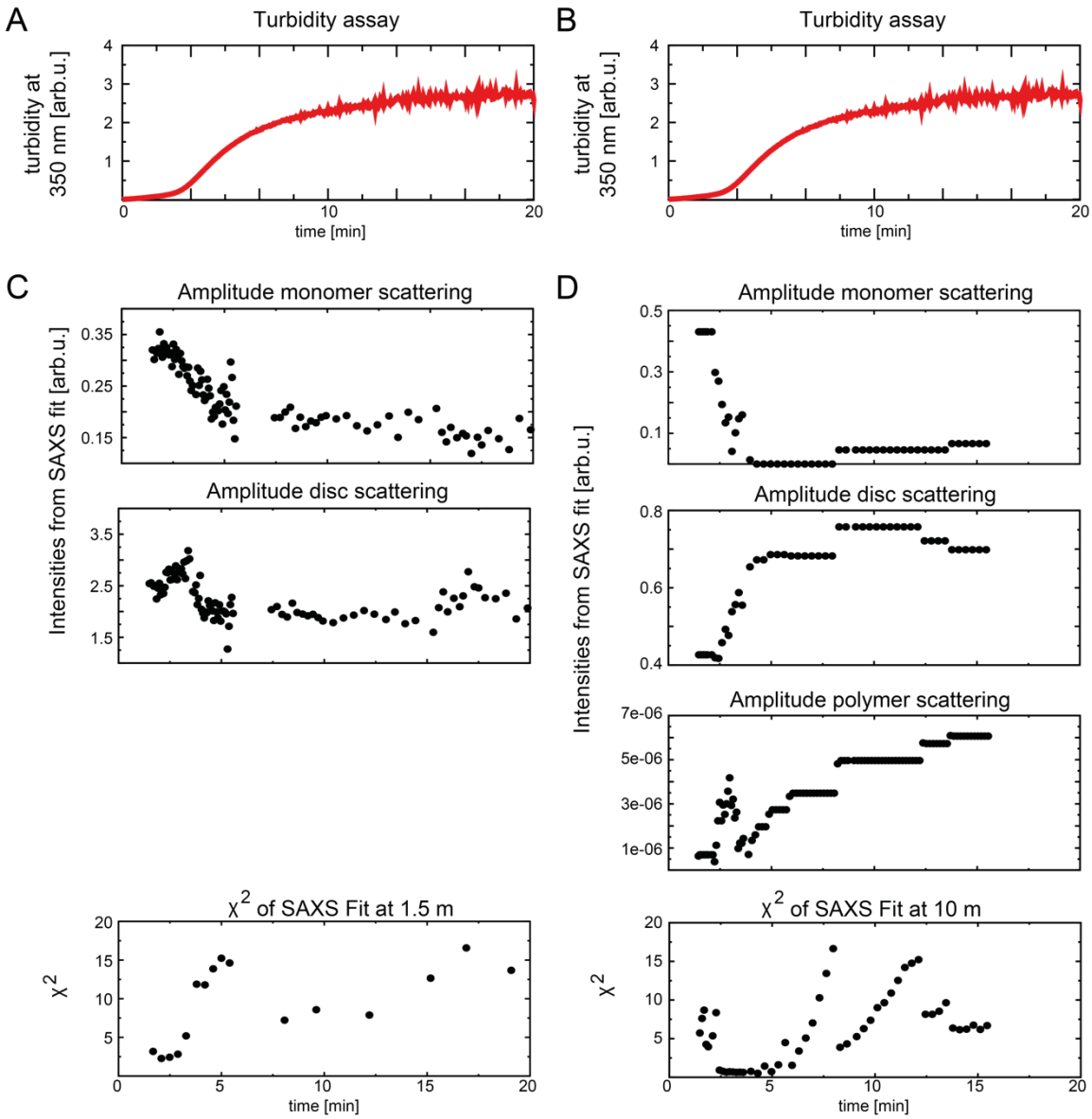

Figure 6-14: Comparison of time-dependent changes in turbidity experiments and of SAXS fit parameters obtained from linear combination of populations model. (**A**)/(**B**) Turbidity change of farn-hGBP1 after nucleotide addition monitored at 350 nm in the upper panels. Both showing 15 μM farn-hGBP1 with 1 mM GDP AlFx in red. (**C**) Amplitude changes of the components included in the SAXS fit to describe the experimental data of 35 μM farn-hGBP1 with GDP AlFx at a detector distance of 1.50 m. Upper panel is showing amplitudes of the monomeric protein and in the second row of the disc-like structures. Last row is indicating the χ^2 values of the fit results. (**D**) Amplitude changes of the components included in the SAXS fit to describe the experimental data of 35 μM farn-hGBP1 with GDP AlFx at a detector distance of 10 m. Upper panel is showing amplitudes of the monomeric protein, second row of the disc-like structures and third row for polymer scattering contributions. Last row is indicating the χ^2 values of the fit results.

The obtained polymer amplitudes from the linear combination of populations fit to the SAXS data, as well as the turbidity curves, are fitted with a Boltzmann's growth fit model as shown in Figure 6-15.

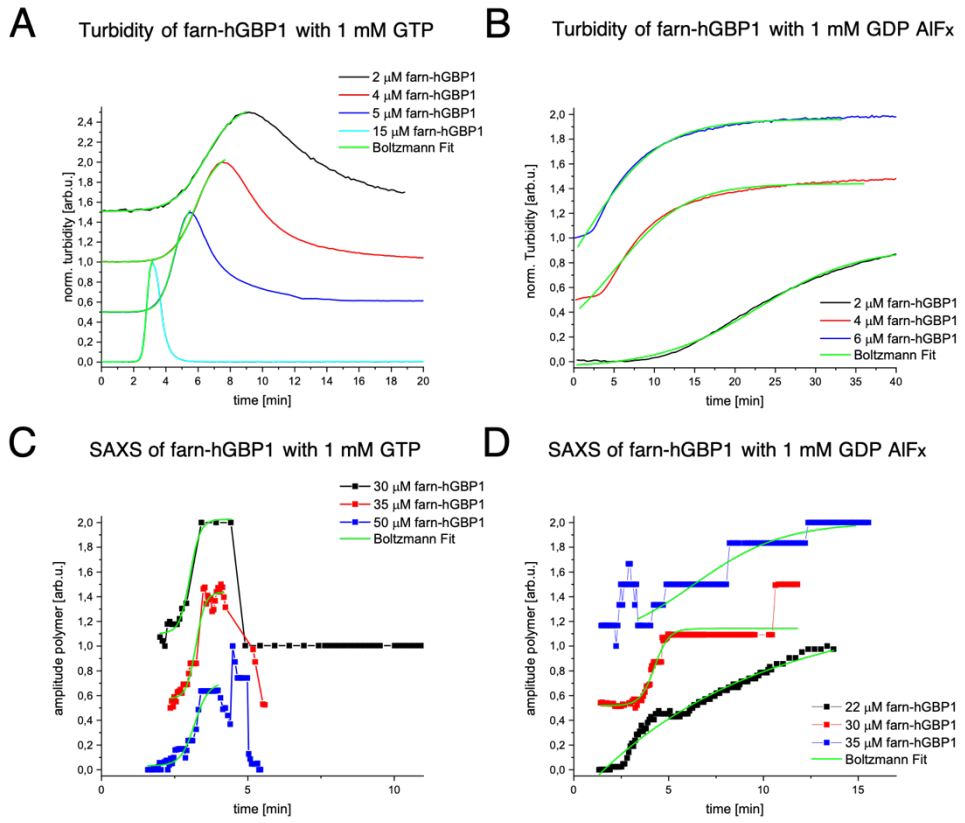

Figure 6-15: Boltzmann Fits of farn-hGBP1 polymerization after nucleotide addition. (**A**) Turbidity assays of 2-15 μM farn-hGBP1 after addition of 1 mM GTP. (**B**) Turbidity assays of 2-6 μM farn-hGBP1 after addition of 1 mM GDP AlFx. (**C**) Polymer amplitudes extracted from SAXS fit of linear combination of populations over time of 30-50 μM farn-hGBP1 after addition of 1 mM GTP. (**D**) Polymer amplitudes extracted from SAXS fit of linear combination of populations over time of 22-35 μM farn-hGBP1 after addition of 1 mM GDP AlFx.

The obtained half-times are extracted and plotted vs. monomer concentration of farn-hGBP1 for both conditions, polymerization after GTP and after GDP AlFx addition respectively (Figure 6-16). The observed polymerization induced by GTP is several orders of magnitudes faster as can be seen from the scale in Figure 6-16 A. Interestingly,

the SAXS derived half times are systematically higher than expected in the case of GTP addition, which was already observed and discussed earlier. From the slope and curvature of the double-logarithmic half-times plot, additional hints into the aggregation mechanism are expected[16]. The scaling exponents of 1.28 +/- 0.19 for GTP-induced polymerization and 0.66 +/- 0.12 for GDP AlFx-induced polymerization are significantly different, thereby implying different underlying aggregation mechanisms. On the other hand, the observed polymer structures from imaging experiments do not suggest a very coordinated and organized higher order structure.

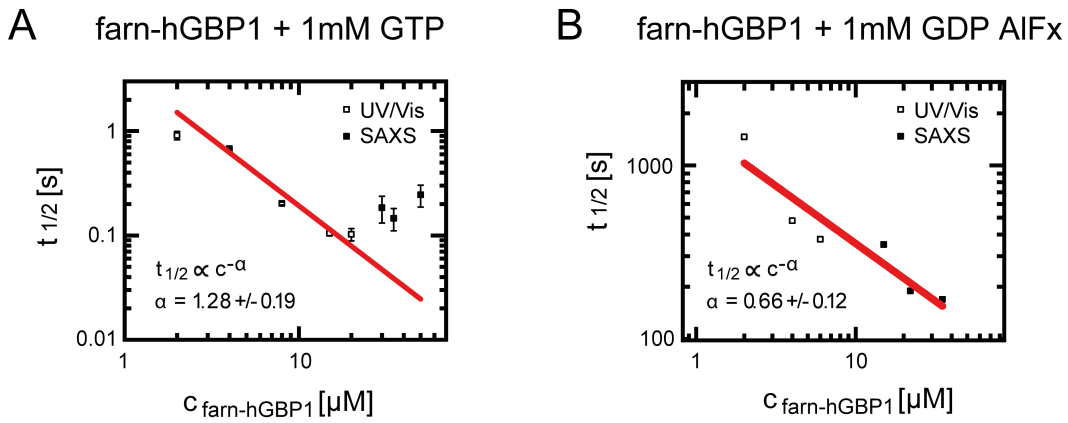

Figure 6-16: Half-times obtained from Boltzmann fits of DLS and SAXS data plotted vs. farn-hGBP1 monomer concentration for polymerization after GTP addition (A) or GDP AlFX addition (B).

This observation of unorganized polymer networks is further underlined by the power law exponent of about 3 to 3.5 that is obtained from SAXS data fits for the polymer scattering behavior. As described by Hammouda[17] and shown in Figure 6-17, the power law exponent of around 3 to 3.5 is characteristic for a clustered network, whereas linear cylinder stacks would yield an expected power law exponent of 1 and are therefore very unlikely to be present under our observed conditions.

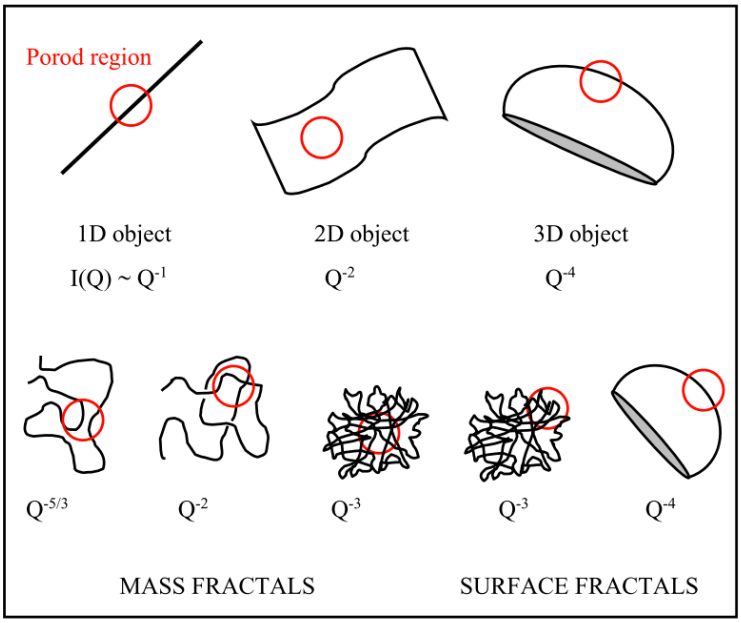

Figure 6-17: Power law scattering behavior of fractal systems and surface objects. The length scale as probed by small angle scattering with X-rays or neutrons is indicated by red circles. The scattering intensity of the shown objects is proportional to a power law of Q with the corresponding exponents given below the objects. (adapted from Hammouda 2016[17])

The comparison of the obtained fit results of the disc's inner structure with the EM results shows that both methods yield similar over all dimensions of the disc with a maximal radius of about 30 nm in both cases. The electron density profile from SAXS measurements was determined using scattering data from 1.50 m detector distance of the measurement with highest farn-hGBP1 concentration in presence of GDP AlFx (35 μM farn-hGBP1), leaving the radii of the shells and their corresponding electron densities as free-floating parameters. For all following fits, those evaluated electron density profiles were fixed and only the height and the amplitude of scattering were left as free parameters, to minimize the degrees of freedom during the fit routines. As seen from Figure 6-10 and Figure 6-11, this approach leads to satisfying fit results even at higher q ranges for other protein concentrations as well, indicating that the shape of the built disc-like structures is protein-concentration independent.

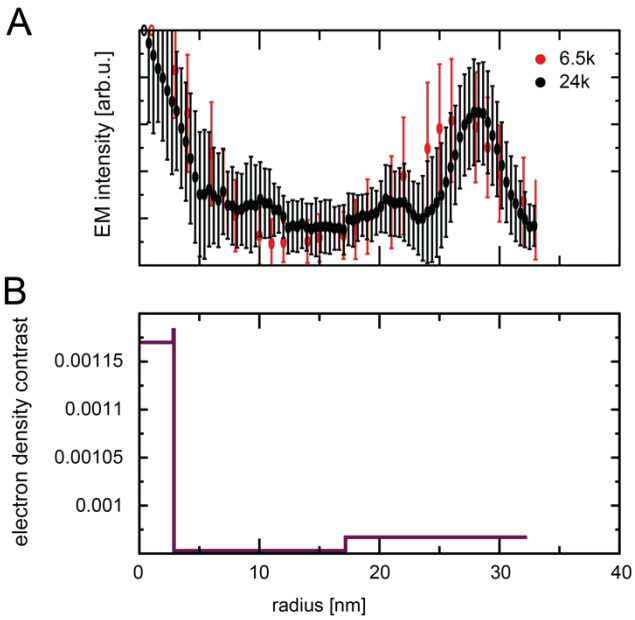

Figure 6-18: Comparison of disc parameters obtained from cryo TEM and SAXS data fitting. (**A**) Averaged density profile of disc-like structures from cryo TEM. (**B**) Electron density profile of the fitted disc-like structures obtained from SAXS data fitting of 35 μM farn-hGBP1 with 1 mM GDP AlFx.

6.4 Discussion

This combination of real space information with time resolved scattering data shows the complementarity of cryo TEM with SAXS leading to cross-validated and refined structural models. We have shown that the oligomerization behavior of farn-hGBP1 is fundamentally different from the unmodified protein that was studied earlier and described in chapter 3 and 5 of this thesis. In contrast to the earlier hypothesized hydrolysis mechanism of hGBP1 cycling between inactive monomers to dimers and eventually tetramers, farn-hGBP1 assembles to large supramolecular clusters upon trapping of the hydrolysis intermediate state using GDP AlFx. From cryo TEM and fluorescence imaging, these clusters seem to be randomly oriented and interconnected, not linearly stacked as proposed earlier[9].

An important additional information would be the formation of the discs during the first 80 seconds that could not be determined from our experiments so far. It would help to understand if the mechanism is related to the observed dynamics as described for the

unmodified protein and therefore also including additional precursors like dimers and tetramers. Moreover, precisely timed kinetic measurements especially after addition of GTP are needed, as the experiments performed in this thesis are all based on manual mixing and timing and therefore, a high experimental error of the time measurements is likely. This is problematic mainly for GTP-induced assembly of farn-hGBP1, as the kinetics are several orders of magnitude fast than after addition of GDP AlFx. An automated mixing setup like mixing chambers or stopped-flow instruments would be beneficial to improve the time resolution and should be performed in a next step.

6.5 Contributions

Charlotte Lorenz (CL) prepared samples for all measurements, planed and performed all experiments and analyzed all measurements. CL wrote the chapter.